Advanced Modelling of ATF Chromium-Coated Zr-Based Cladding High Temperature Oxidation

Alexander Vasiliev
Nuclear Safety Institute (IBRAE)
Moscow, Russia
vasil@ibrae.ac.ru
ORCID 0000-0002-1587-1648

***Abstract*— Currently, the use of special low-corrosion coatings on nuclear reactors claddings made of zirconium-based alloys is considered as one of encouraging ways to strengthen the reliability and performance of nuclear fission generation. This milestone direction of development is an evolutional way in nuclear power plants (NPPs) development. The chromium seems to be one of the best materials for protective coating.**

The chromium has excellent characteristics of corrosion and oxidation resistance compared to zirconium both for the NPP normal operation temperatures and high-temperature conditions. It is very important for the nuclear safety including the resistance to beyond-design-basis and design-basis accidents at NPPs. However, recent experimental data showed that in the temperature range close to upper limit of design-basis accident (1200°C) and higher there is a considerable worsening of *Zr/Cr* cladding protective properties. In particular, a role of *Cr-Zr* interdiffusion with subsequent influence on degradation of protective properties is revealed.

In this paper, the new advanced model of high-temperature oxidation of *Zr/Cr* cladding is developed based on simultaneous solution of oxygen and zirconium diffusion equations in different layers of the cladding. In particular, a very important role of *Zr* outward diffusion to the interface between chromium oxide and metallic chromium resulting to severe degradation of protective properties is discovered recently. This phenomenon is taken into account in the model. The model is implemented to newly developed numerical module.

The predictions of the model are compared with some experimental results on *Zr*/*Cr* claddings high-temperature oxidation available in the literature. The comparison shows that the basic phenomena are modeled with reasonable accuracy.

Keywords—nuclear power plant, advanced tolerant fuel Zr/Cr cladding, chromium coating, high-temperature oxidation, theoretical model, computer-running numerical program

I. INTRODUCTION

The search for perspective ATF (advanced tolerant fuel) materials including new types of claddings for new generation nuclear reactors is underway throughout the world [1-5]. New materials for claddings should demonstrate exclusively high corrosion and oxidation resistance and applicable neutronic characteristics.

The zirconium-based alloys with chromium coating of thickness in the range 5÷20 μm have been determined as one of the most promising candidates for use in ATF-claddings [6-11]. *Cr* is generally deposited on the *Zr* surface using a process of Physical Vapor Deposition (PVD).

The existing data show that Zr/Cr cladding has excellent parabolic oxidation kinetics which is at least one order of magnitude lower if we compare it with standard zirconium-based claddings. Definitely, it is valid for normal operation conditions and for design basis accidents with temperatures not exceeding 1200°C.

The possible application of *Zr*-based claddings with chromium coating in commercial NPPs presupposes the preservation of other positive characteristics of *Zr*-based claddings are retained (high melting temperature, low absorption cross-section of thermal neutrons, good plasticity *etc*.).

However, recent experimental data [6,10,11] discovered that outstanding oxidation resistance properties relevant of *Zr/Cr* cladding experience a considerable worsening when approaching temperatures about 1200°C, that is, significantly lower than the melting point of chromium. This is due to a number of factors:

- The protective properties of growing oxide layer are gradually worsened due to formation of cracks and pores in the oxide layer. It takes place in particular in the course of mechanical stress development in oxide layer under oxidation conditions. The reason of this phenomenon is connected with the difference of molar volumes of *Cr* and Cr_2O_3 (the Bedworth-Pilling ratio). The formation of cracks and pores in chromium oxide layer will result in the enhancement of effective oxygen diffusion coefficient in this layer;
- The Cr_2Zr intermetallic compound layer with a thickness of about several microns is formed between zirconium and chromium layers. *Zr* atoms diffuse into the metallic chromium coating layer resulting in progressive growth of the precipitates of ZrO_2 inside this layer. In this turn, it leads to enhancement of effective oxygen diffusion coefficient in chromium layer, because the diffusion is stronger along the ZrO_2 grain boundaries;
- When *Zr* atoms migrate through metallic *Cr* layer to rich Cr_2O_3/*Cr* interface, the redox reaction of *Zr* with Cr_2O_3 begins resulting to formation of ZrO_2 and *Cr*. So, this reaction leads to thinning of Cr_2O_3 layer and to growth of metallic *Cr* layer. Obviously, the protective properties will gradually worsen once again due to thinning of protective Cr_2O_3 layer.

In this paper, the basic equations of advanced *Zr/Cr* cladding oxidation model are considered describing the phenomena mentioned above. The involvement of different physical-chemical processes important for overall cladding behavior depends on the current characteristic phase of oxidation. The corresponding numerical computer-running program is developed. The comparison of model predictions with the results of recent experimental tests conducted in KAERI, Korea and KIT, Karlsruhe, Germany, both for the

temperature T=1200°C, is given. Finally, the main conclusions are made on the basis of results obtained.

II. Basic Equations of Zr/Cr Cladding High Temperature Oxidation and Approaches to Modelling

On the basis of experimental results [6], one can see several phases of *Zr/Cr* cladding oxidation which will progressively develop in time in the course of accident. We consider the upper limit of design-basis accident temperature T=1200°C.

The first or initial phase (Phase I) is an oxidation in a two-layer system Cr_2O_3/Cr, see Fig. 1. During this phase, the oxygen will not reach the underlying *Zr* substrate. Due to exceptional oxidation characteristics of chromium, a very low rate of oxidation is expected at this phase. The simple parabolic oxidation law is applicable.

The next phase (Phase II) of oxidation assumes the gradual transition from the first phase with low kinetics to the state when the protective properties of chromium layer will be almost completely lost due to a number of factors. The oxidation kinetics is getting stronger during this phase and is not parabolic.

Finally, we encounter the final phase of oxidation (Phase III). The protective properties of chromium coating are exhausted at this phase and the oxidation of *Zr* substrate with formation of ZrO_2 layer is observed. The oxidation kinetics is parabolic again but displays much higher coefficient.

In the beginning, let us consider the oxidation at Phase I. To calculate the diffusion of oxygen in the cladding we consider the schematics shown in Fig. 1.

We are looking for a solution of the following diffusion equations in each of two layers Cr_2O_3 and *Cr*:

$$\frac{\partial^2 c_O}{\partial x^2} = \frac{1}{D}\frac{\partial c_O}{\partial t}, \qquad (1)$$

where c_O is the oxygen density [kg/m^3], D – the oxygen diffusion coefficient in the corresponding layer, t – the time. The initial and boundary conditions for c_O at external and interphase boundaries should be applied. Also, the diffusion flux continuity at all boundaries should also be taken into account.

The approximate solution of Eq. 1 is given on the basis of paper [12] by the following way:

$$\delta_{Cr_2O_3} = \sqrt{k_p t} = K_{ox}\sqrt{t}\,, \qquad (2)$$

$$\frac{K_{ox}}{\sqrt{4D_{ox}}} \approx \cong \frac{\left[\sqrt{\frac{4c_{md}\cdot c_{md}}{\pi} + 8\frac{D_{ox}}{D_m}\left(c_{\frac{d}{m}} - c_{\frac{m}{d}}\cdot r\right)\cdot\left[c_{\frac{d}{O}} - c_{\frac{d}{m}}\right]} - \frac{2c_{\frac{m}{d}}}{\sqrt{\pi}}\right]}{4\sqrt{\frac{D_{ox}}{D_m}}\cdot\left(c_{\frac{d}{m}} - c_{\frac{m}{d}}\cdot r\right)}, \qquad (3)$$

where K_{ox} – the parabolic constant, D_{ox} and D_m – oxygen diffusion coefficients in Cr_2O_3 and *Cr* layers respectively, $c_{d/O}$, $c_{d/m} \cong c_{d/O}$ and $c_{m/d}$ – the parameters in Fig. 1 from *Cr-O* phase diagram. The Bedworth-Pilling ratio is $r = r_{Cr} = \left(\rho_{Cr_2O_3}/\rho_{Cr}\right)\cdot\left(2\mu_{Cr}/\mu_{Cr_2O_3}\right)$, ρ and μ - the densities and molar weights of corresponding substances. The parameter $c_{m/d}$ is much less than $c_{d/m}$ which means a low solubility of oxygen in metal *Cr*.

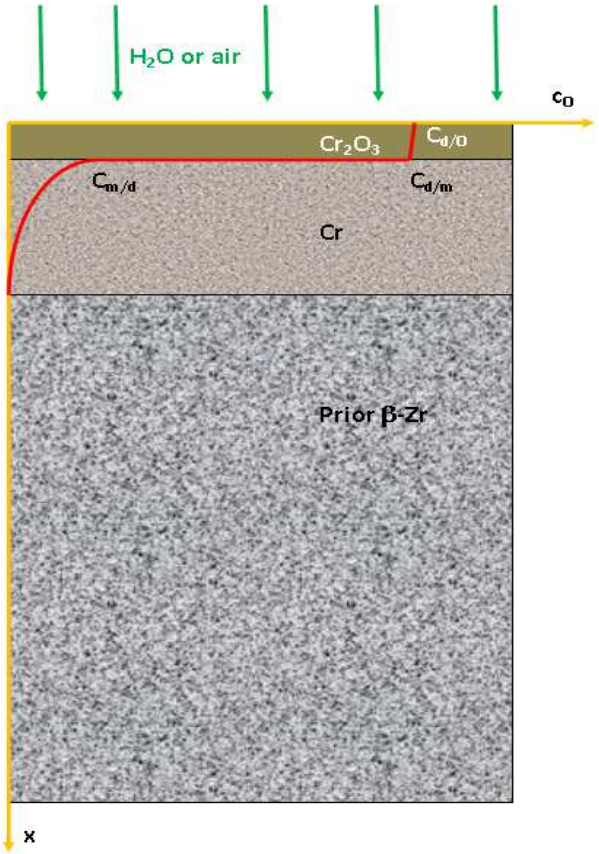

Fig. 1. Phase I. The profile of oxygen concentration

We can estimate the constant $k_p = K_{ox}^2$ by

$$k_p = 4.83\cdot 10^{-5}\cdot e^{-\frac{31228}{T}}\ \text{m}^2/\text{s}\,, \qquad (4)$$

on the basis of the experimental data [6].

So, the constant K_{ox} is given below:

$$K_{ox} = 6.95\cdot 10^{-3}\cdot e^{-\frac{15614}{T}}\ \frac{m}{\sqrt{s}}\,. \qquad (5)$$

The protective layer of Cr_2O_3 is rigid and dense at this phase I. It means that the oxidation kinetics is parabolic. For example, the dependence of weight gain dynamics on time at temperature T=1200°C is presented in Fig. 2 (blue line). The dynamics of ZrO_2 layer thickness during Zircaloy-4 cladding oxidation is given in this Fig. 2 for comparison (black line).

One can note a huge difference (almost two orders of magnitude) in weight gain behavior between these claddings. But this behavior is typical only for Phase I.

The Fig. 3 shows the calculated dependence of oxygen concentration profile in *Zr/Cr* cladding on time during oxidation of chromium at the temperature T=1473K. We see how the oxygen profile in the cladding is evolved in time.

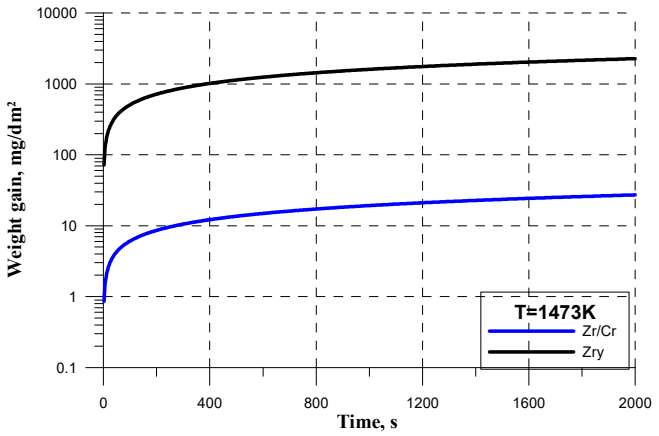

Fig. 2. Dynamics of weight gain for uncoated (*Zry*) and coated cladding (Zr/*Cr*) at *T*=1473K

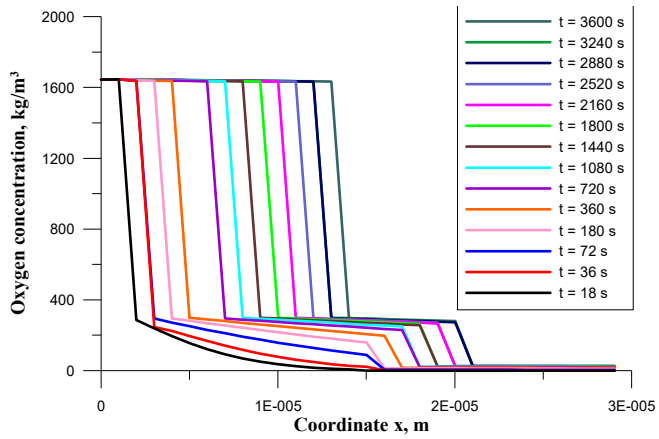

Fig. 3. Dynamics of oxygen concentration profile in time for Zr/Cr cladding during oxidation at *T*=1473K

Now we turn to Phase II. The transient phase begins at time *t* about 200 s after the oxidation beginning at temperatures about 1200°C.

This phase is characterized by consecutive enhancement of oxidation rate. On the one hand, the important reason for such behavior is the growth of effective oxygen diffusion coefficient *D* in Cr_2O_3 layer (in the process of Cr_2O_3 layer spallation and a formation of cracks and pores in it, see Fig. 4). On the other hand, the enhancement of effective oxygen diffusion coefficient *D* in *Cr* layer also takes place but by another reason, Namely, it is due to enhancement of diffusion along growing *Zr* dioxide precipitates grains boundaries because the diffusion is often much stronger along the grain boundaries in the solid.

The formation of ZrO_2 in Cr_2O_3 is caused by diffusion of zirconium into the chromium layer and further to the boundary between the layers of chromium oxide and metallic chromium leading to redox reaction $3Zr+2Cr_2O_3=3ZrO_2+4Cr$;

Also, the atoms of *Cr* from Cr_2O_3 are replaced by *Zr* atoms which result in redox reaction $3Zr+2Cr_2O_3=3ZrO_2+4Cr$. So, the protective chromium oxide layer is diminished in thickness. As a result, we see the gradual increase of oxygen diffusion flux to underlying prior *Zr*.

The main equations describing these phenomena are written as follows. The oxygen diffusion flux through Cr_2O_3 layer is equal to

$$J_O = D_{ox}\frac{(c_{d/O}-c_{d/m})}{\delta_{Cr_2O_3}}. \quad (6)$$

Then, the numerical routine to calculate the chromium oxide thickness dynamics $\delta_{Cr_2O_3} = d$ in time is written below:

$$d^{n+1} = d^n + K_{d1}\tau - J_{cr}^n\frac{n\tau}{\rho_{Cr_2O_3}}, \quad (7)$$

where

$$J_{Cr} = \frac{4}{3}J_{Zr}\ , J_{Zr} = -D_{Zr}A/d_{Cr}\ , K_{d1} = \frac{J_O\mu_{Cr_2O_3}}{\mu_O\rho_{Cr_2O_3}}. \quad (8)$$

The upper subscript *n* in variable d^n denotes the number of time step τ. The parameter K_{d1} describes the oxide thickness increment during one timestep, J_{Zr} – the zirconium diffusion flux through metallic chromium layer, J_{Cr} – the chromium flux from the Cr_2O_3 layer to the *Cr* layer due to redox reaction, d_{Cr} – the metallic chromium layer thickness, *A* – the empirical constant.

Finally, consider now the Phase III. As we understand from above-mentioned discussion at this phase there are no more obstacles for oxygen to penetrate into the *Zr* metal layer. It means that we have a classical oxygen diffusion problem in two-layer (ZrO_2/α-*Zr(O)*) or three layer system (ZrO_2/α-*Zr(O)*/β-*Zr*) depending on temperature *T*. For *T*= 1200°C we encounter the three-layer system for zirconium, see Fig. 4.

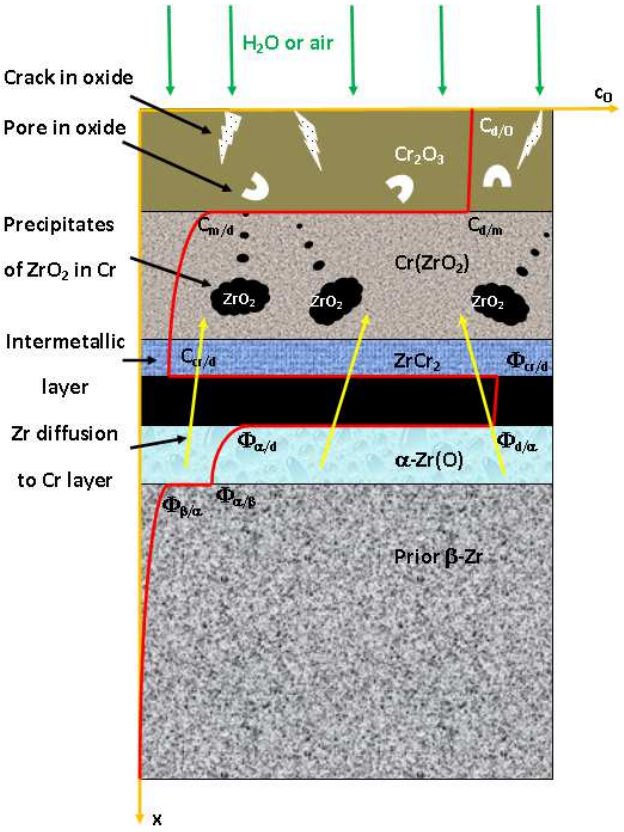

Fig. 4. Phases II and III. Oxygen concentration profile in the cladding when both Cr_2O_3 oxide layer and the *Cr* metallic layer already lost their protective functions. The ZrO_2 layer is represented as a black one

As in the case of Phase I we should solve the following oxygen diffusion equations:

$$\frac{\partial^2 c_O}{\partial x^2} = \frac{1}{D_i}\frac{\partial c_O}{\partial t}, \qquad (9)$$

but now in three layers ZrO_2, α-$Zr(O)$ and β-Zr with corresponding diffusion coefficients D_i. As previously, all conditions at external and interphase boundaries must be fulfilled.

The approximate dynamics of parameters δ_d (the thickness of ZrO_2 layer) and δ_a (the sum of ZrO_2 layer thickness and of α-$Zr(O)$ layer thickness) are represented as [12]:

$$\delta_d = K_d\sqrt{t}\,,\ \delta_a = K_a\sqrt{t}\,, \qquad (10)$$

$$\frac{K_a}{\sqrt{4D_a}} \cong 1, \qquad (11)$$

$$\frac{K_d}{\sqrt{4D_d}} \cong$$

$$\cong \frac{-\left(\Phi_{\frac{\alpha}{d}} - \Phi_{\frac{\alpha r}{\beta}}\right)\sqrt{\frac{D_a}{D_d}} + \sqrt{\left(\Phi_{\frac{\alpha}{d}} - \Phi_{\frac{\alpha r}{\beta}}\right)^2 \frac{D_a}{D_d} + 8A^2\left(\Phi_{\frac{d}{\alpha}} - \Phi_{\frac{\alpha r}{d}}\right)\left(\Phi_{\frac{d}{\bar{\alpha}}} - \Phi_{\frac{d r}{\alpha}}\right)}}{4A\left(\Phi_{\frac{d}{\alpha}} - \Phi_{\frac{\alpha r}{d}}\right)},$$

$$\mathrm{A} = \int_0^{\frac{K_a}{\sqrt{4D_a}}} e^{-y^2} dy.$$

Once again, among the parameters is $r = r_{Zr} = \left(\rho_{ZrO_2}/\rho_{Zr}\right)\cdot\left(2\mu_{Zr}/\mu_{ZrO_2}\right)$ (Bedworth-Pilling ratio for Zr-ZrO_2 system); the physical dimension of the oxygen interface concentration Φ is [kg/m^3], see Fig. 4.

Note, that the solutions (10,11) are also the parabolic dependencies as in the case of chromium oxidation but with much more large coefficient. It is obvious that we treat the case without the protective chromium coating.

III. Results of Modelling

Below are presented the results of numerical modelling compared to recent experimental results, see Figs. 5a, 5b and 7.

One of first experimental example of nonlinear (non-parabolic) behavior during Zr/Cr cladding oxidation was the paper [12]. In this paper, the isothermal steam oxidation of cladding made from Zircaloy-4 alloy with chromium coating was investigated at the temperature T=1473K. The thickness of Cr coating was 10 μm.

Note that only outer surface of Zry cladding had a Cr coating in the experiment. The inner surface of cladding was prior Zry.

The model developed in this paper was used for calculation of weight gain dynamics in the course of the experiment. We suppose that the transient phase of oxidation (Phase II) was begun at t = 400 s after the start of experiment. So, the linear enhancement of effective oxygen diffusion coefficient D_i (i – the name of corresponding layer) for both chromium oxide and metal chromium layers in time is supposed in calculations beginning from the time t=400 s and till the time time t=2000 s (the end of experiment and calculation). Totally, the effective oxygen diffusion coefficient D was enlarged by 16 times in the end.

Such enhancement corresponds to the growth of parabolic parameter K_{ox}, see Eq. 2, by about four times (square root from 16) to the end of test. We can say that the parameter $K_{diff}=D_{ox,eff}/D_{ox}$ (the enhancement factor of oxygen diffusion coefficient) was 16.

The results of numerical calculations are presented in Fig. 5a. We can clearly see the initial parabolic dependence which after some time goes to transition phase (Phase II) and finally to oxidation of prior Zircaloy substrate. The calculation for uncoated Zry cladding is also given in this Figure for comparison. It is expected, that if we extrapolate those graphs to longer times, the red curve should approach to the black one.

The experimental dependencies are reproduced in Fig. 5b. The comparison between calculated end experimental dynamics demonstrates the good agreement.

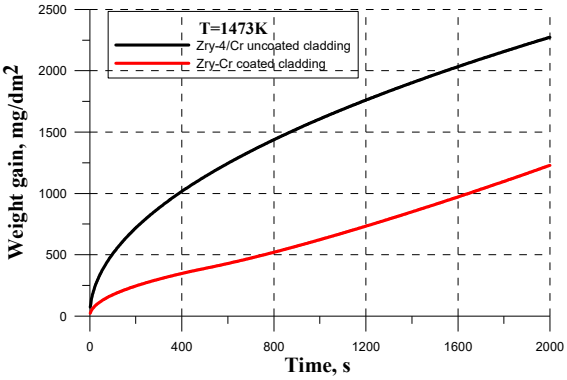

Fig. 5a. The results of weight gain calculated by numerical module

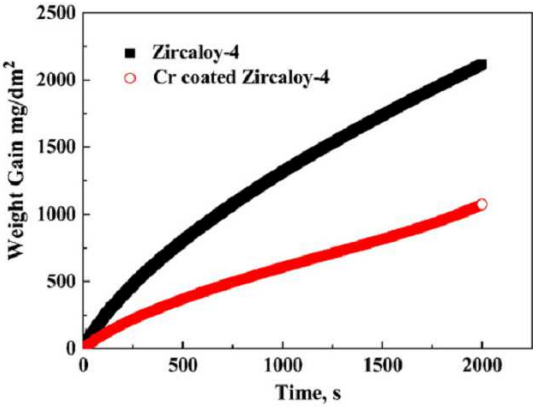

Fig. 5b. The cladding weight gain in the course of the experiment. The graphs are reproduced from the paper [12]

The investigation of the influence of parameter K_{diff} (the enhancement factor of oxygen diffusion coefficient in chromium oxide layer) on chromia thickness dynamics in time is presented in Fig. 6. The parameter K_{diff} is determined as $K_{diff}=D_{ox,eff}/D_{ox}$ that is the ratio of effective (enhanced) oxygen diffusion coefficient in chromium oxide layer to a standard value of D_{ox}. The enhancement of D_{ox} is due to formation of cracks and pores in chromia layer, see Fig. 4.

It is seen from Fig. 6 that the enhancement factor K_{diff} as large as 5.4 leads to acceleration of oxidation dynamics by

about two times. These results are in agreement with analytical results presented in Fig. 5a.

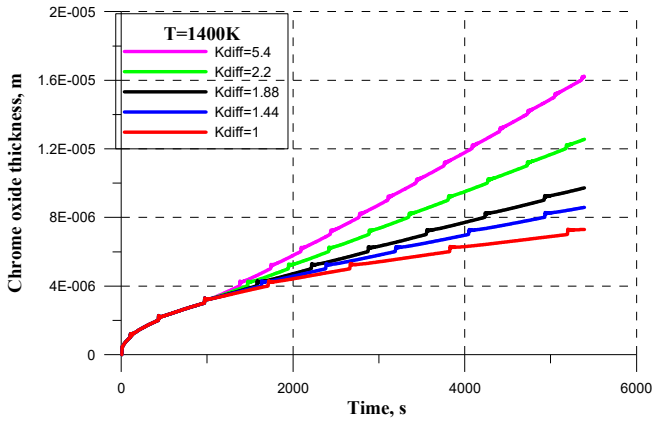

Fig. 6. The calculated dependence of Cr_2O_3 layer thickness on time with different parameter K_{diff} at the temperature T=1400K

The isothermal experiment [8] with *Cr*-coated *Zry*-4 cladding oxidation conducted recently at KIT, Karlsruhe, Germany, is chosen for modelling. The experimental data clearly show the initial growth of Cr_2O_3 layer (Phase I, t=0÷2000 s). Then, the thinning of Cr_2O_3 layer is observed (Phase II, t=2000÷7200 s). The calculated and experimental data are presented in Fig. 7.

We see that new code developed in this paper predicts the experimental behavior pretty well taking into account the incredibly complicated nature of this process. The second term in right hand of Eq. 6 ensures the initial parabolic growth of chromium oxide layer. Then, the third term in right hand of Eq. 6 begins to prevail and we come to diminishing the chromium oxide layer. Correspondingly, the oxygen flux to the sample increases leading to transition from parabolic to linear oxidation kinetics (Phases II and III). The ZrO_2 layer begins to form (observed in this experiment) which means the loss of protective properties of chromium-coated *Zry*-4 cladding.

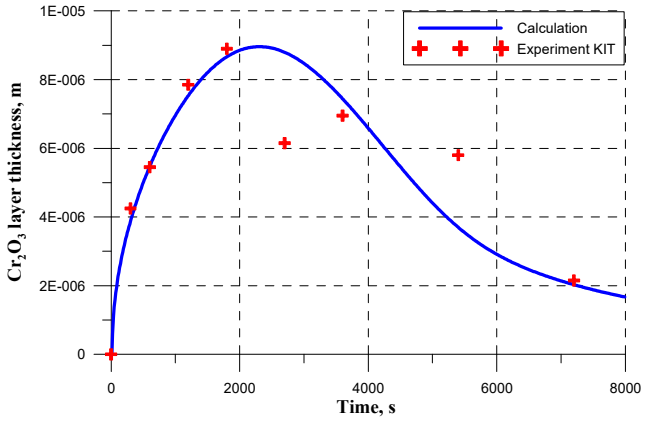

Fig. 7. Chromium oxide thickness: the results of numerical calculation (blue line) compared to experimental dynamics (KIT, Karlsruhe) reproduced from the paper [8]. The temperature T=1200°C

IV. Conclusions

In this paper, the basic analytical approaches to model high-temperature oxidation of ATF-cladding *Zr/Cr* are presented. This very complicated process needs the detailed consideration including many physical and chemical aspects.

The weight gain parabolic oxidation kinetics of ATF Zr/Cr cladding is presented in Fig. 8. One can see, that zirconium-based claddings with chromium coating can be a good candidate material for future NPPs. The considerable enhancement of NPPs safety is expected.

The recent experimental data discovered that the gradual loss of protective properties of chromium coating takes place during oxidation at high temperatures (1200°C and above). This circumstance may lead eventually to the loss of protective properties of chromium coating.

The advanced analytical model of *Zr/Cr* cladding is developed in the paper on the basis of existing understanding and recent available experimental investigations throughout the world. The processes which are attendant the high-temperature oxidation of *Zr/Cr* cladding occur to have a complicated physical-chemical nature and require a detailed modeling. The model was implemented to numerical computer-running program.

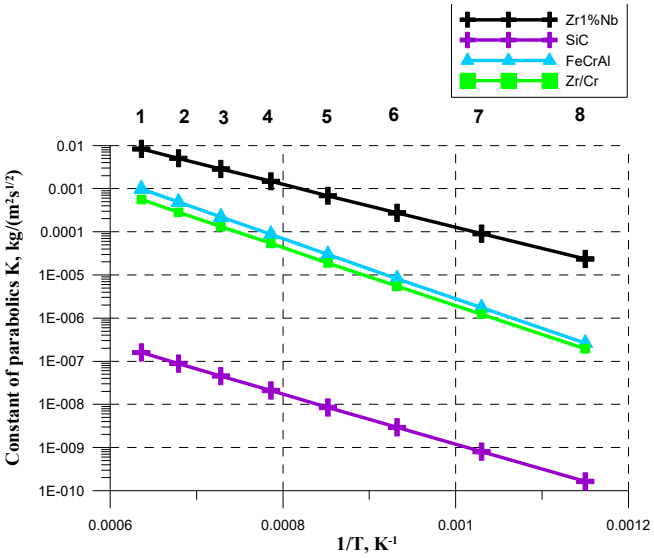

Fig. 8. Parabolic oxidation kinetics of Zr/Cr cladding in comparison with other perspective ATF-claddings for future NPPs. The data from papers [13-15] are used

To check out the predictive ability of developed model for *Zr/Cr* cladding high temperature oxidation, the comparison between calculated data and some experimental data (KAERI, Korea and KIT, Karlsruhe, Germany) for the temperature T=1200°C is performed. One can note the reasonable agreement between calculated and experimental results.

On the whole, the use of ATF *Zr/Cr* claddings in nuclear reactors is justified due to the providing additional time to mitigate the consequences of postulated design-basis accidents. Depending on a scenario, the gain in time may be as much as 2÷6 hours. Also, there is a good probability to avoid the escalation to severe accident phase.

The deterioration of protective properties of the *Zr*/*Cr* claddings revealed in experiments at temperatures of 1200°C and above encourages researchers to search for various modifications of protective coatings. For example, the paper [11] considers bilayer *Cr*/*Mo* coating instead of *Cr* monolayer for use on *Zr*-alloy claddings. The first encouraging data on this coating's protective properties are obtained in the above-mentioned paper. It means that the analytical modelling of such complicated coatings will be also necessary in nearest future.

Currently, the search for other materials for coatings on Zr-based NPP fuel claddings is in progress throughout the world with the aim to enhance protective properties at higher temperatures 1200°C and above.

ACKNOWLEDGMENT

The author would be glad to acknowledge the colleagues from KIT, Karlsruhe, Germany, involved in reactors severe accidents investigations for the valuable discussions on the topic.

REFERENCES

[1] Terrani, K.A. Accident Tolerant Fuel Cladding Development: Promise, Status, and Challenges. J. Nucl. Mater. 2018, 501, 13–30. https://doi.org/10.1016/j.jnucmat.2017.12.043.

[2] Qiu, B.; Wang, J.; Deng, Y.; Wang, M.; Wu, Y.; Qiu, S.Z. A Review on Thermohydraulic and Mechanical-Physical Properties of SiC, FeCrAl and Ti3SiC2 for ATF Cladding. Nucl. Eng. Technol. 2020, 52, 1–13. https://doi.org/10.1016/j.net.2019.07.030.

[3] Ott, L.J.; Robb, K.R.; Wang, D. Preliminary Assessment of Accident-Tolerant Fuels on LWR Performance during Normal Operation and under DB and BDB Accident Conditions. J. Nucl. Mater. 2014, 448, 520–533. https://doi.org/10.1016/j.jnucmat.2013.09.052.

[4] Wagih, M.; Spencer, B.; Hales, J.; Shirvan, K. Fuel Performance of Chromium-Coated Zirconium Alloy and Silicon Carbide Accident Tolerant Fuel Claddings. Ann. Nucl. Energy 2018, 120, 304–318. https://doi.org/10.1016/j.anucene.2018.06.001.

[5] Chen, H.; Wang, X.; Zhang, R. Application and Development Progress of Cr-Based Surface Coatings in Nuclear Fuel Element: I. Selection, Preparation, and Characteristics of Coating Materials. Coatings 2020, 10, 808. https://doi.org/10.3390/coatings10090808.

[6] J.-Ch. Brachet, E. Rouesne, J. Ribis, T. Guilbert, S. Urvoy, G. Nony, C. Toffolon-Masclet, M. Le Saux, N. Chaabane, H. Palancher, A. David, J. Bischoff, J. Augereau, E. Pouillier, "High temperature steam oxidation of chromium-coated zirconium-based alloys: kinetics and process", Corrosion Science, vol. 167, 108537, 15 pp, 2020. https://doi.org/10.1016/j.corsci.2020.108537.

[7] P. Vrbka, J. Krejci, J. Kabatova et al., "Air oxidation of sponge based E110 cladding alloy at high temperatures", Proc. 23th International QUENCH Workshop (QUENCH-23), Karlsruhe, Germany, October 17-19, 2017.

[8] J. Liu, U. Stegmaier, C. Tang, M. Steinbrueck, M. Grosse, "The coating degradation mechanism during the isothermal steam oxidation of Cr-coated Zry-4 at 1200°C", Proc. 26th International QUENCH Workshop (QUENCH-26), Karlsruhe, Germany, December 6-10, 2021.

[9] A. Vasiliev, "High-temperature oxidation modeling of new perspective accident tolerant fuel claddings", Proc. 2019 ASME International Mechanical Engineering Congress and Exposition (IMECE2019), Salt Lake City, Utah, US, IMECE2019-10513, November 11-14, 2019. https://doi.org/10.1115/IMECE2019-10513.

[10] J.-H. Park, H.-G. Kim, J.-Y. Park, Y.-I. Jung, D.-J. Park, Y.-H. Koo, "High temperature steam-oxidation behavior of arc ion plated Cr coatings for accident tolerant fuel claddings", Surface & Coatings Technology, vol. 280, pp. 256-259, 2015.

[11] M. Syrtanov, E. Kashkarov, A. Abdulmenova, K. Gusev and D. Sidelev, "High-temperature steam oxidation of accident-tolerant Cr/Mo-Coated Zr Alloy at 1200-1400°C", Coatings, vol. 13, 191,17 pp, 2023. https://doi.org/10.3390/coatings13010191.

[12] A. D. Vasiliev, "Advanced model of Zr-based claddings oxidation in steam-oxygen-nitrogen gas mixtures embracing all range from low to high temperatures", Proc. SAFEST Air Oxidation Meeting "Cladding Oxidation by Air under Severe Accident Conditions in a Nuclear Reactor and a Spent Fuel Pool", Budapest, Hungary, June 14-15, 2016.

[13] B.A. Pint, K.A Terrani, M.P. Brady, T. Cheng, J.R. Keiser, "High Temperature Oxidation of Fuel Cladding Candidate Materials in Steam–Hydrogen Environments", J. Nucl. Materials, 2013, V. 440, P. 420–427.

[14] K.G. Field, M.A. Snead, Y. Yamamoto, K.A. Terrani, "Handbook on the Material Properties of FeCrAl Alloys for Nuclear Power Production Applications", ORNL/SPR-2018/905, US, August 2018.

[15] J.H. Baek, K.B. Park and Y.H. Jeong, "Oxidation Kinetics of Zircaloy-4 and Zr-1Nb-1Sn-0.1Fe at Temperatures of 700-1200°C", J. of Nuclear Materials, 2004, V. 335, P. 443-456.